J. Biophotonics **6**, No. 2, 188–196 (2013) / **DOI** 10.1002/jbio.201200016

Journal of BIOPHOTONICS

FULL ARTICLE

Intercoupling surface plasmon resonance and diffusion reflection measurements for real-time cancer detection

*Rinat Ankri, Amihai Meiri, Shemuel I. Lau, Menachem Motiei, Rachela Popovtzer, and Dror Fixler**

Faculty of Engineering and the Institute of Nanotechnology and Advanced Materials, Bar Ilan University, Ramat Gan, 52900, Israel

Received 5 February 2012, revised 12 March 2012, accepted 12 March 2012
Published online 2 April 2012

Key words: gold nanoparticles, gold nanorods, inter-particle coupling, molecular imaging, red-shift, spatial diffusion reflection, cancer detection

Spatial diffusion reflection (DR) measurements of gold nanorods (GNR) were recently suggested as a simple and highly sensitive non-invasive and non-ionizing method for real-time cancer detection. In this paper we demonstrate that wavelength dependent DR measurements enable the spectral red-shift observation of highly concentrated GNR. By conjugating targeting moieties to the GNR, large density of GNR can specifically home onto cancer cells. The inter-particle plasmon resonance pattern of the highly concentrated GNR leads to an extension and a red-shift ($\Delta\lambda$) in the absorption spectrum of the concentrated GNR. Dark-field microscopy was used in order to measure the expected $\Delta\lambda$ in different GNR concentrations *in vitro*. Double-wavelength DR measurements of tissue-like phantoms and tumor bearing mice containing different GNR concentrations are presented. We show that the DR profile of the highly concentrated GNR directly correlate with the spectral extension and red-shift. This presented work suggests that wavelength dependent DR method can serve as a promising tool for real-time superficial tumor detection.

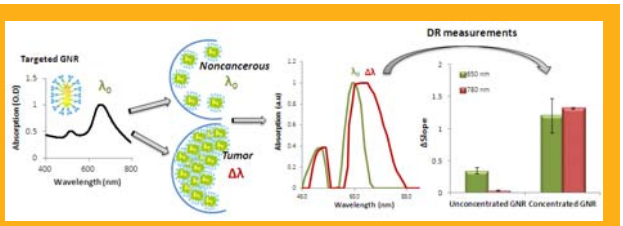

Targeted GNR, with $\lambda_0 = 650$ nm, accumulate in the tumor while the noncancerous tissue contains a lower GNR concentration. Double-wavelengths diffusion reflection measurements selectively detect the tumor as the inter-particle plasmon resonance pattern of the highly concentrated GNR leads to an extension ($\Delta\lambda$) and a red-shift in the absorption spectrum of the concentrated GNR in tumor.

1. Introduction

The Diffusion Reflection (DR) based medical imaging is very attractive since it is non-ionizing, low cost, convenient to generate and detect, and highly sensitive to the optical properties of the tissue. This non-invasive method is based on the measurement and investigation of the reflected light intensity (defined as Γ) profile of an irradiated tissue in several light source-detector separations (defined as ρ). The $\Gamma(\rho)$ profile is influenced by the tissue optical properties, such as its absorption and scattering coefficients (μ_a and μ_s, respectively) and the anisotropy factor g. Whereas μ_a is mainly related to tissue's

* Corresponding author: e-mail: Dror.Fixler@biu.ac.il, Phone: 972-3-5317598, Fax: 972-3-7384051

chromophores [1, 2], μ_s and g reflect the form and concentration of the scattering components in the irradiated tissue [3, 4]. As the biological tissue is defined as a turbid three-dimensional medium, the scattering property of the tissue is usually defined by the reduced scattering coefficient, μ_s', calculated by the following equation:

$$\mu_s' = (1-g)\,\mu_s \tag{1}$$

Numerous researches presented the influence of the tissue's optical parameters on the light path within the tissue. These include the effect of anisotropic optical properties on the photon migration [5], the time of flight and photon path length for photons in tissues using the radiation transfer equation [6] and the penetration depth in irradiated tissue [7–9]. The knowledge of these properties is necessary for optimizing techniques such as near-IR (NIR) spectroscopy, photodynamic therapy, etc.

During the last decade, several diagnostic methods were developed based on DR measurements. Thus, for e.g., Yang et al., 2001 [10] suggested UV reflectance spectroscopy for DNA and protein changes probing in human breast tissues. Zhu et al., 2006 [11] have presented diagnosis of breast cancer using DR spectroscopy, while a physical model (Monte Carlo inverse model) and an empirical model (partial least squares analysis) based approach were compared for extracting diagnostic features from the diffuse reflectance spectra. Cerussi et al., 2011 [12] presented diffuse optical spectroscopic imaging (DOSI) as a non-invasive and quantitative method which enables the measurement of tissue hemoglobin, water and lipid. Still, as many other spectroscopic methods, the DR technique suffers from multiple scattering which dominates light propagation in tissue. Therefore, a diagnostic tool which can diminish the scattering interruption on the DR signal is desired.

In our previous works [13, 14] we have demonstrated that gold nanorods (GNR) can highly influence the absorption properties of the irradiated tissue. We measured $\Gamma(\rho)$ from several tissue-like phantoms and tumor bearing mice and showed that it was proportional to the absorption properties of the GNR. As the GNR can be specifically targeted to tumor cells, such as squamous cell carcinoma (SCC) head and neck cancer (HNC) cells, the DR measurements were proved to be a highly sensitive tumor detection tool. We have also proved that the DR profile of the tissue is correlated to its optical properties by the simple description [14]:

$$\Gamma(\rho) = \frac{c_1}{(\rho)^2}\exp(-\mu\rho) \tag{2}$$

While c_1 is a constant, depending on the optical properties of the medium and the sizes of the light source and detector apertures. μ is the effective attenuation coefficient given by (for $\mu_a \ll \mu_s'$) [15, 16]:

$$\mu = \sqrt{3\cdot\mu_a\mu_s'} \tag{3}$$

Equation (3) suggests that the exponential decay of $\Gamma(\rho)$ equally depends on the tissue reduced scattering and absorption coefficients. As certain sizes of GNR can present high absorption but very low scattering [17], by their insertion to the irradiated tissue one can increase the absorption properties of the tissue whereas the scattering coefficient remains the same. Thus, the absorption influence on the DR signal increases and μ can be defined by Eq. (3) (since the tissue still presents $\mu_a < \mu_s'$).

In the present study, we suggest the utilization of the Surface Plasmon Resonance (SPR) coupling effect between adjacent GNR and the resulted red-shift in their absorbance spectra [18–21] for tumor detection based on DR measurements. SPR coupling, also known as inter-particle coupling [22], is a phenomenon in which the resonance wavelength peak of two interacting nanoparticles is generally red-shifted (to a lower photon energy) compared to the resonance wavelength of a single nanoparticle [22, 23]. This red-shift in the gold nano partials absorption spectrum was previously used for tumor detection based on photoacoustic imaging [19, 24]. In this paper, we suggest that this shift in the GNR absorption spectrum can be used as a highly sensitive DR method for SPR coupling based tumor detection. The GNR can be selectively targeted to HNC tumor and form an exclusive concentrated assembly of those GNR in the SCC cancer cells [25]. Thus, highly concentrated GNR will be created only in the tumor while the non-cancerous tissue will present much lower concentrations of GNR. In the present work, the DR method ability to identify SPR coupling in GNR was demonstrated using tissue-like solid phantoms. *In-vivo* DR measurements of tumor-bearing mice following different concentrations of intravenous injected GNR are presented and the SPR coupling detection is demonstrated.

2. Materials and methods

2.1 The optical set-up

Double-wavelength DR measurements were performed, where the first wavelength correlates with the absorption peak of the suspended GNR and the second wavelength correlates with the expected extension and red-shift ($\Delta\lambda$) of the absorption spectrum. For this purpose, a noninvasive optical technique was designed and built for reflected light intensity measurements [13, 26]. The set-up included

two laser diodes, with wavelengths of 650 and 780 nm, which were optically bundled to a split fiber (125 μm diameter) for irradiation. A portable photodiode, deposited at different distances ρ on the samples' surface, served as a detector, enabling DR intensity (Γ) measurements in several light-source detector separations (symbolized as $\Gamma(\rho)$). The photodiode's cross-section diameter was 1 mm^2. The initial distance ρ between the light source and the first location of the photodiode was ∼1 mm. A micrometer plate, to which the optic fiber was attached, enabled a consecutive reflected light intensity measurement. The micrometer plate was moved in 21 incremental steps of 250 μm each. The reflected light intensity was collected from 1 mm (the initial distance between the light source and the photodiode) to 6.25 mm. The reflected intensity $\Gamma(\rho)$ (in Voltage) was collected using a digital scope (*Agilent Technologies, Mso7034a, Santa Clara, CA*) as well as a DAQ (USB-6008, National Instruments, Israel). The data was processed using the MATLAB (the Mathworks Inc., 2010) and LabView (National Instruments, 2009) softwares.

2.2 Gold nanorods fabrication

Two sizes of GNR, presenting absorption spectra in 650 and 780 nm, were prepared and the DR method ability to distinguish between their different SPRs was proved. The GNR were synthesized using the seed mediated growth method [27]. Their size, shape and uniformity were characterized using transmission electron microscopy (TEM) (Figure 1) and presented a narrow size distribution (10%). The absorption spectra of the GNR solutions were measured and are presented in Figure 1 (left side). Two kinds of GNR were synthesized: the first, named as GNR_{650}, have average dimensions of 65×25 nm, resulting in an aspect ratio ($\equiv R$) of 2.6 and an average effective radius (r_{eff}) of 19 nm [17]. These GNR presented an absorption peak at 650 nm and their TEM picture is presented in the upper right side of Figure 1. The second kind of GNR, named as GNR_{780}, presented average dimensions of 52×13 nm, resulting in $R = 4, r_{\text{eff}} = 12.5$ nm and an absorption peak at 780 nm. Their TEM picture is presented in the lower right side of Figure 1. According to Jain et al., 2006 [17], these GNR have high absorption properties at 650 and 780 nm but much less dominant scattering properties: while GNR_{650} are expected to have an absorption coefficient 3 times higher than their scattering coefficient, GNR_{780} are expected to present an absorption about 14 times higher than their scattering coefficient.

Only GNR_{650} were used for the *in-vivo* measurements in order to illuminate with 780 nm laser, according to the expected spectral red-shift. The GNR_{650} antibody conjugation and the zeta potential measurements are described in details in our previous works [13, 14].

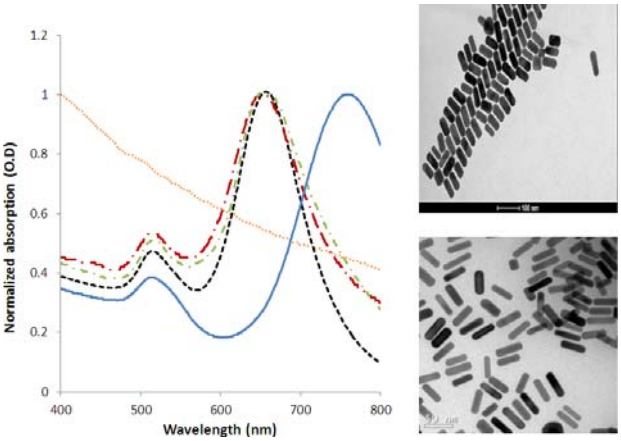

Figure 1 (online color at: www.biophotonics-journal.org) Left: UV-Vis absorption spectra (normalized) of 3% India ink (dotted line) bare GNR_{650} (25×65 nm, thin dashed line), PEG coated (thick dashed line) and Anti-EGFR coated (dot-dashed line) GNR_{650} and GNR_{780} (52×13 nm, solid line). Right: TEM images of the bare GNR_{650} (up) and GNR_{780} (bottom).

2.3 Solid phantoms preparation

Solid phantoms were prepared and simulated the skin tissue optical properties [28]. The phantoms were prepared using 3×10^{-3}% of India Ink, as an absorbing component, 2% of Intralipid (Lipofundin MCT/LCT 20%, B. Braun Melsungen AG, Germany) as a scattering component [29] and 1% Agarose powder (SeaKem LE Agarose, Lonza, USA), in order to convert solution into a gel. We determined the absorption spectrum of the India ink (see Figure 1, dotted line) using a spectrophotometer and calculated the absorption coefficient (μ_a) of each phantom according to the concentration of the ink in each solution. The scattering properties of the phantoms were experimentally determined in our previous work [14]. The resulted μ_a of the phantoms was 0.0137 mm^{-1} and the reduced scattering coefficient (μ_s') was ∼1.45 mm^{-1}.

Into six identical phantom solutions, GNR_{650} (4 mg/mL) were added to achieve final concentrations of 0.01, 0.02, 0.05, 0.1, 0.15 and 0.2 mg/ml of gold. In addition, GNR_{780} (4 mg/mL) were added to another phantom and presented a final concentration of 0.02 mg/ml.

All phantom solutions were heated and mixed at a temperature of approximately 90 °C while the Agarose powder was slowly added. All phantom solutions were poured into a 24 wells plate (each well

with a 16 mm diameter) and were cooled under vacuum conditions (to avoid bubbles).

2.4 Dark-field reflectance imaging

Dark field reflectance images of GNR_{650} were captured using the hyper spectral imaging system (Nuance, CRi, MA, USA). A Xenon illumination, along with a 40× dark field objective (0.75 NA) and 32-bit ultrasensitive CCD camera detector (N-MSI-EX, CRi, MA, USA) were used for imaging in a RGB mode. Microscopy then was performed on a Nikon 80i Microscope (Nikon instruments, Inc). Images were acquired using the Nuance software version 2.1. In dark field microscopy, a very narrow beam of white light is delivered on top of the sample. The large scattering angle allows detection of highly scattering objects (such as GNR, due to their enhanced SPR) with a very little background signal. We prepared three different concentrations of GNR_{650} solutions as three volumes of 5, 12 and 20 µl were taken from a solution presenting 3.1 mg/ml of GNR_{650}. The resultant densities of the GNR_{650}, on slides with dimensions of 1 cm^2, were 0.0155, 0.0372 and 0.062 mg/cm^2.

2.5 In-vivo experiment

In-vivo DR measurements were evaluated using mice bearing human HNC derived from an A-431 SCC cell line. A-431 cells (2×10^6) were injected subcutaneously into the back flank area of 10–11 week-old nude mice.

Two concentrations of GNR_{650} were injected into two groups of mice: group 1 received 200 µl of ~10 mg/ml while group 2 received 200 µl of ~30 mg/ml. When the tumor reached a size of five to seven millimeters in diameter, the mice received the GNR_{650} by tail vein injection. Mice tumor and normal tissue were scanned before GNR_{650} injection and ~16 hours post injection. Diffusion reflection measurements were performed on three to five different sites on the mice's skin.

All *in-vivo* measurements were performed under appropriate anesthesia: the mice barrier-controlled facility was under the strict care of the veterinarian in charge of the Institutional Animal Care and Use Committee (IACUC). The mice were inspected daily by the veterinarian, who handles the appropriate tests and treatment protocols, as required. All research protocols were followed closely by the veterinarian. All major procedures were performed in the surgical facilities using general anesthesia and standard, aseptic surgical techniques.

3. Results

3.1 DR measurements of Solid phantoms containing GNR

DR measurements of solid phantoms containing both, GNR_{650} and GNR_{780}, were performed using the

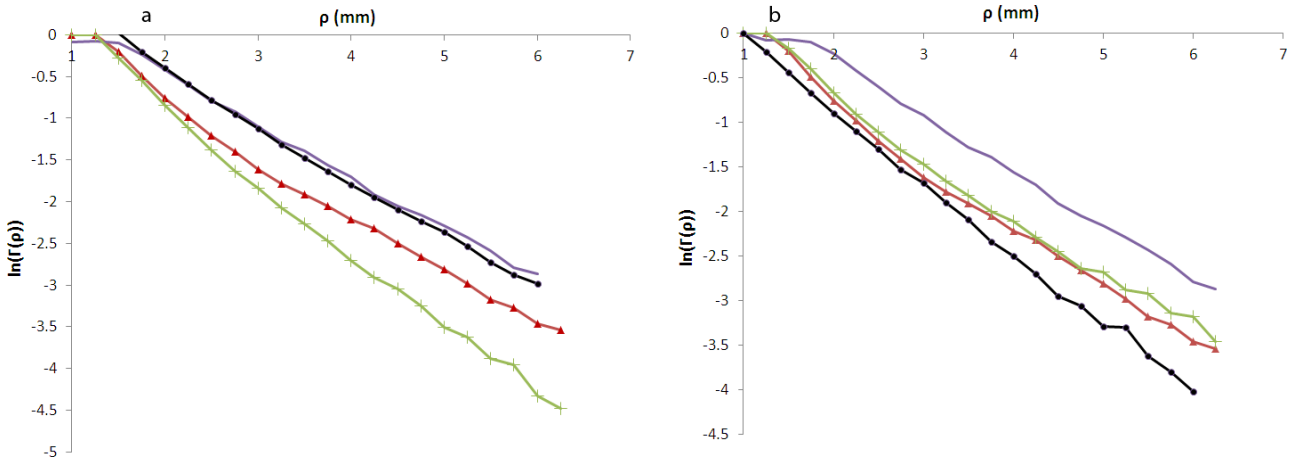

Figure 2 (online color at: www.biophotonics-journal.org) Diffusion reflection intensities (in semi-logarithmic scale), as a function of the distance between the detector and the light source, of different phantoms as follows: (**a**) a homogeneous phantom with a reduced scattering property of $\mu_s' \sim 1.45\ mm^{-1}$, and $\mu_a = 0.0137\ mm^{-1}$ following 650 and 780 nm illuminations (the triangle marked and the solid line, respectively) and a solid phantom containing 0.01 mg/ml GNR_{650} following 650 and 780 nm illuminations (the cross and circle marked lines, respectively) (**b**) the same homogeneous phantom following 650 and 780 nm illumination (the triangle marked and the solid line, respectively) and solid phantom containing 0.02 mg/ml GNR_{780} following 650 and 780 nm illuminations (the cross and circle marked lines, respectively).

experimental set-up described above. Representative results of the reflected light intensity profiles of a phantom with 0.01 mg/ml of GNR_{650} are presented in Figure 2(a). The experimental results correlate well with the predicted behavior: first, the solid phantom without GNR (named as a *homogeneous phantom*) presents a DR profile with a more negative slope following 650 nm illumination compared to 780 nm illumination (the slopes were 0.69 and 0.60 for the triangle marked and solid lines, respectively). This is in a good correlation with the ink absorption spectrum presented in Figure 1, which shows a higher absorption in the 650 nm. Second, while the 650 nm illumination results in a more negative slope (of 0.87, the cross marked line in Figure 2(a)) than the homogeneous phantom, the phantom that was illuminated with 780 nm kept a constant slope before and after the 650 nm illumination.

Figure 2(b) presents similar results for 780 nm illumination of a phantom containing 0.02 mg/ml of GNR_{780}. While the DR curve following 780 nm illumination presented an increase in its DR slope compared to the phantom without GNR (the slopes values of the circle marked and solid lines were 0.79 and 0.60, respectively), the DR curve following 650 nm illumination remained the same (a slope 0f 0.63, the cross marked line in Figure 2(b)). As mentioned in the *Materials and methods* section above, these GNR present high absorption properties at 650 and 780 nm but much less dominant scattering properties. Therefore, the observed increase in the graphs' slopes is due to the increase in the absorption of the irradiated phantom, resulting from the presence of the GNR. These results suggest that our detection method can observe different sizes of GNR (based on their different SPRs).

Figure 3 presents the Δ slopes of all irradiated phantoms, calculated from their DR profiles. The Δ slope is defined as the difference between the DR slopes of a phantom with GNR_{650} and a homogeneous phantom. It is well seen that for low GNR concentrations (0.01 and 0.02 mg/ml in Figure 3) the DR profiles present the predicted behavior, as the Δ slopes present significant values following 650 nm illumination only (0.19 ± 0.02 and 0.34 ± 0.05 for 0.01 and 0.02 mg/ml, respectively). Starting from 0.05 mg/ml, the Δ slopes following 780 nm illumination became significant, resulting in 0.45 ± 0.04, 0.88 ± 0.21, 1.3 ± 0.18 and 1.31 ± 0.27 for 0.05, 0.1, 0.15 and 0.2 mg/ml of GNR_{650}, respectively. The resulted Δ slopes following 650 nm illumination present similar values of 0.58 ± 0.2, 0.75 ± 0.21, 1.29 ± 0.18 and 1.19 ± 0.27 for the same concentrations, respectively. This similarity in the Δ slopes following both wavelengths irradiation, despite the fact that the phantoms contained GNR_{650} only, indicates that a red-shift and peak expansion occur in the GNR absorption spectrum. In order to identify this spectral red-shift, dark-field microscopy was used.

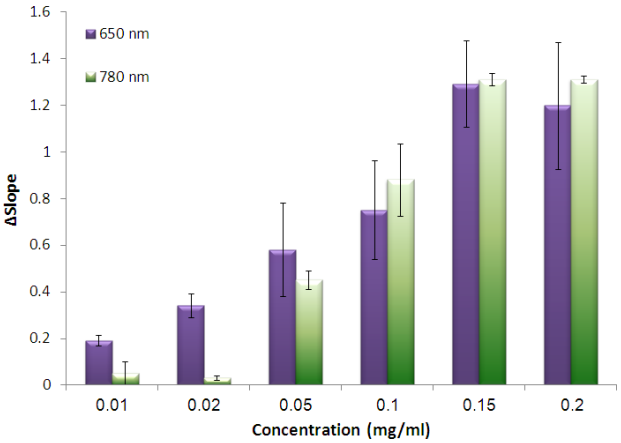

Figure 3 (online color at: www.biophotonics-journal.org) Comparison between the reflected light intensity Δ slopes (absolute values) of the phantoms containing GNR_{650} following 650 and 780 nm illuminations. The results are the average of diffusion reflection measurements of different phantoms. The error bars represent error of the mean.

3.2 In vitro dark-field reflectance imaging of different GNR concentrations

Different concentrations of GNR_{650}, according to the description in the *Materials and Method* section above, were measured using the dark-field microscopy and their total absorption spectra were collected. The resulted absorption spectra of two different densities, 0.0155 and 0.0372 mg/cm^2, are presented in Figure 4. The dashed curve shows the absorption spectrum of GNR_{650} in a relatively low density on the slide, of 0.0155 mg/cm^2. This spectrum well correlates the absorption properties of the GNR_{650} suspended in water (the dashed line in Figure 1), presenting a colloidal suspension with high spacing between particles, therefore no red-shift is observed ($\Delta\lambda = 0$). The dashed-dotted curve is the resulted absorption spectrum of GNR_{650} with a higher density, of 0.037 mg/cm^2. The absorption spectrum still presents the GNR 'fingerprint' peak in 530 nm. Yet, the SPR coupling of the GNR_{650} is well observed as the intense absorption peak shifted to the red region, resulting in an absorption peak of 733 nm ($\Delta\lambda = 83$ nm). A larger red shift (to ~750 nm, $\Delta\lambda = 100$ nm) was observed for GNR_{650} density of 0.062 mg/cm^2 (data not shown). These results indicate that in high densities of GNR_{650}, SPR coupling occurs. It explains the increase in the DR slopes of phantoms presenting high GNR_{650} concentrations following 780 nm illumination.

Still, since the GNR are not homogeneously dispersed on the slide, the total spectrum should include different SPR peaks, of 650 and of several red-shifted peaks toward the 750 nm. Indeed, the dotted

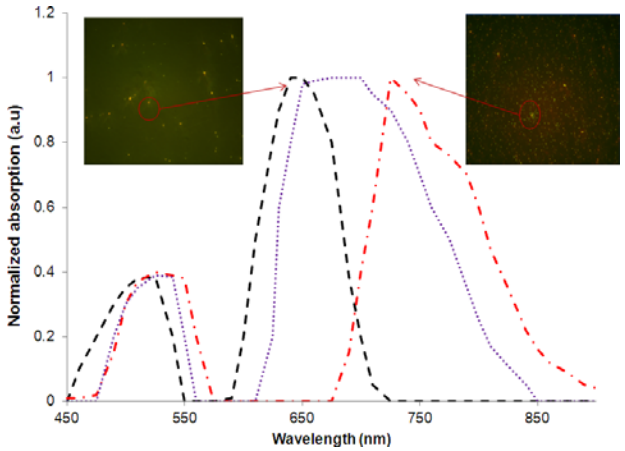

Figure 4 (online color at: www.biophotonics-journal.org) Absorption spectra of a single GNR_{650} from two slides presenting densities of 0.0155 mg/cm^2 (dashed line) and 0.0372 mg/cm^2 (dashed-dotted line). The spectral red-shift of GNR in the higher density was 75 nm. The dotted line represents the broadening in the absorption spectrum of grouped GNR in high densities. Inset: dark-filed microscopy images of 0.0155 mg/cm^2 (left) and 0.0372 mg/cm^2 (right) GNR_{650}.

line in Figure 4 shows a broaden graph which was also observed in high densities of GNR_{650} (0.037 and 0.062 mg/cm^2). The broadening indicates an inhomogeneous dispersion of the nanoparticles, resulted in an ensemble of red shifts (as was also presented by Mallidi et al., 2009 [19]). Since the DR slopes of phantoms containing highly concentrated GNR_{650} increased following both, 650 and 780 nm illuminations, this broadening in the absorption spectrum suggests the appropriate explanation.

3.3 Refractive index influence on the GNR SPR

It was previously reported that a change in the refractive index of the gold nano particles' surrounding might change their SPR. In order to ensure that the red-shift and the expansion of the SPR peak observed by the DR measurements result from SPR coupling, the discrete dipole approximation (DDA) method [30] has been exploited. We performed the DDA simulations using the freely available DDSCAT 7.0 program [31]. The program enables to calculate the absorption, scattering and extinction cross sections, among other quantities, for targets of arbitrary size and shape, taking into account the wavelength dependent complex refractive index of the material and the refractive index of the surrounding medium. In order to calculate the absorption spectrum of the GNR_{650}, the incident light's polarization was set to be longitudinal and the wavelength in vacuum was between 300 and 1000 nm with 10 nm spacing far from the peak and 1 nm around the peak.

The GNR_{650} SPR was obtained for the refractive index of water (as Figure 1 presents the resultant absorption spectra of GNR suspended in water, $n = 1.33$ [32]), of the phantom (mainly determined by the IL component, $n = 1.36$ [33], which is the same refractive index of skin and muscle [34]) and for six more varying refractive indexes between 1.3 and 1.46. We found that the red shift observed following the GNR_{650} insertion to the phantom solution was 10 nm only, similar to the results presented by Chen et. al, 2008 [32]. These results indicate that the refractive index of the phantoms, as well as of the tumor (which presents a refractive index similar to skin or muscle) do not influence the GNR_{650} SPR. Thus, one can deduce that the Δ slopes presented in Figure 3 do indicate the SPR coupling occurred in phantoms containing high concentrations of GNR_{650}.

3.4 In-vivo DR measurements of tumor bearing mice

The tumor-bearing mice were irradiated, under appropriate anesthesia, and the reflected light intensity was measured using the optical set-up described above. The reflectance measurements were performed before the GNR_{650} injection and ~16 hours post-injection. The slopes of the reflected light intensity profiles were calculated and representative results are shown in Figure 5.

Figure 5(a) presents the DR profiles of the tumor bearing mice, group 1. As was mentioned in the *Materials and methods* section, this group received a relatively low concentration of GNR_{650}. Indeed, the DR spectra present the same behavior observed for phantoms containing low concentrations of GNR_{650} as the slope of the curve increased following 650 nm illumination only (0.50 ± 0.014 and 0.67 ± 0.02 before and 16 hours post injection, solid and triangle marked lines, respectively), while illumination with 780 nm did not affect the DR slope (an average slope of 0.46 ± 0.042, circle and asterisk marked lines, before and 16 hours post injection, respectively). In contrast, the DR spectra of group 2, shown in Figure 5(b), present the behavior observed for highly concentrated GNR_{650} in phantoms, as the DR curves show an increase in their slope following both 650 (triangle marked line) and 780 nm (asterisk marked line) illuminations compared to their slopes before illumination (solid and circle marked lines, respectively). The average slopes increased from 0.55 ± 0.032 to 0.8 ± 0.009 before and 16 hours post illumination, respectively. These results well indicate

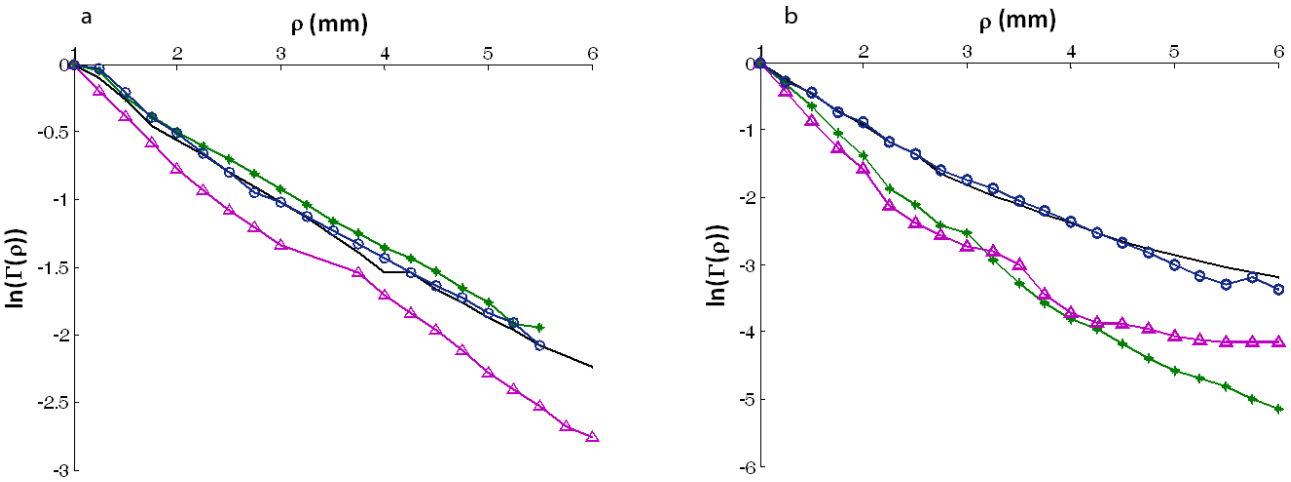

Figure 5 (online color at: www.biophotonics-journal.org) Diffusion reflection intensities (in semi-logarithmic scale) as a function of the distance between the detector and the light source. The graph emphasizes the difference between the slopes before GNR_{650} injection and 16 hours post injection following both, 650 and 780 nm illuminations. (**a**) DR profiles of the cancerous tissue presenting a relatively low GNR_{650} concentration. While the reflectance slope following 780 nm illumination presents the same value as before illumination (circle and asterisk marked lines before and after illumination, respectively), 650 nm illumination introduced a sharper slope (triangle marked line) compare to the slope before the GNR injection (solid line). (**b**) DR profiles of the cancerous and non-cancerous tissues presenting a higher GNR_{650} concentration. The DR profiles of the tumor following 650 and 780 nm illuminations (triangle and asterisk marked lines, respectively) introduced an increase in the curves' slopes compare to the non-cancerous tissue before the GNR_{650} injection (solid and circle marked lines).

that DR measurements can identify a red-shift in tumors in-*vivo* in real time.

4. Discussion

Spatial diffusion reflection measurements with GNR as contrast agents were previously suggested by us to present a simple, inexpensive and highly sensitive diagnostic tool for *in-vivo* cancer detection in real-time [13, 14]. This method is based on the change in the absorption properties of the tumor site following intravenous injection of EGFR targeted GNR. In this work, the spectral red-shift occurs in high concentrations of GNR was suggested to serve as an additional parameter for DR based tumor detection measurements.

In the present study, the SPR coupling in highly concentrated GNR was first observed using DR measurements of phantoms containing different GNR_{650} concentrations. Figure 3 presents the Δ slopes of the logarithmic form of the phantoms' $\Gamma(\rho)$ profiles following 650 and 780 illuminations. It is well observed that the higher is the GNR_{650} concentration, the more intense is the Δ slope following 780 nm illumination. In order to verify whether the observed red-shift of the GNR_{650} in phantoms resulted from SPR coupling only, and not from the difference between the refractive indexes of the water and the phantom, the DDA method [31] was used. The results suggested that a very small red-shift, of $\Delta\lambda \sim 10$ nm, is expected for the GNR_{650} in phantoms or tissues compare to GNR_{650} suspended in water.

The expected spectral red-shift of different concentrated GNR_{650} was calculated from *in-vitro* measurements, using the dark-field microscopy. The results, shown in Figure 4, present a spectral red-shift of $\Delta\lambda = 83$ nm in high densities of GNR_{650}. This shift was observed while single GNR (each surrounded by other GNR) were detected. As for a group of GNR, an expansion of the absorption peak was observed, indicating an inhomogeneous dispersion of the GNR. Figure 3 indicates this broadening in the absorption spectra, as in high concentrations of GNR_{650} the DR slope increased almost identically following both, 650 and 780 nm illuminations. If only a red-shift occurred, the DR slopes should introduce an increase in the DR slopes following 780 nm illumination only.

Figure 5 presents real-time DR measurements of two groups of tumor bearing mice. The two groups presented different GNR_{650} concentrations in tumor 16 hours post GNR_{650} injection. This delay time was chosen since in our previous work it was found that for >10 hours post the GNR injection their accumulation in tumor was sufficient for their detection using our DR set-up [13]. The results indicate a behavior similar to the observed behavior in Figure 3: the DR measurements of group 1, which received a low concentration of GNR_{650}, showed an increase in

Early View publication on
www.wileyonlinelibrary.com
(issue and page numbers not yet assigned;
citable using Digital Object Identifier – **DOI**)

their slopes following 650 nm illumination only, indicating that no red-shift occurred in the accumulated GNR in tumor. In contrast, DR measurements of group 2 presented an increase in the DR slope following both, 650 and 780 nm illuminations, suggesting a broadening of the SPR toward the red wavelengths range.

These results serve as a preliminary study of SPR coupling based DR measurements for tumor detection. Intravenous administration of targeted GNR results either in a specific binding between the EGFR-targeted GNR and the cancer cells (like SCC), or the inevitable non-specific distribution in the blood and other organs. Further investigation is required in order to demonstrate our ability to distinguish between non-specific and specific (targeted) binding of the functionalized nanoparticles based on their spectral shift. Targeted GNR will present a $\Delta\lambda$ in the tumor site due to their specific attachment to the HNC cells resulting in an inter-particle coupling effect. If there are no cells of interest in the sample, the measured resonant wavelength peak will be the same as of a single GNR. Thus, by screening the skin tissue with a double-wavelength DR set-up, the tumor can be detected. A similar red-shift based tumor detection method was suggested by Mallidi et al., 2009 [19], named as multiwavelength photoacoustic imaging, enabling the detecting and differentiating of cancer cells labeled with anti-EGFR gold nanoparticles from the endogenous chromophores. Still, in this method a high pulse repetition rate laser and ultrasound detector are used, which are highly expensive and much more sophisticated equipment. The DR method can provide a simpler and highly sensitive tool for the detection of superficial tumors such as head and neck cancer, breast cancer and melanoma.

In conclusion, this paper demonstrated in tissue-like phantoms and *in-vivo* mice model that DR imaging can detect the spectral red-shift and the peak broadening that occur in highly concentrated GNR. Based on the results presented in this paper, further investigation is desired on superficial tumor models to determine the optimal concentration of the specifically targeted GNR as well as the sufficient delay time post injection, which are required to obtain sufficient absorption contrast in DR imaging.

Acknowledgements We thank Ivan Charamisinau for making available his program for Mie theory calculations of composite particles and B. T. Draine and P. J. Flatau for use of their DDA code, DDSCAT 7.1. This research was also partly supported by a grant (code no. 05K1501–02110) from the "Center for Nanostructured Materials Technology" under "21st Century Frontier R & D Programs" of the Ministry of Science and Technology, Korea.

Author biographies Please see Supporting Information online.

References

[1] J. W. Feather, D. J. Ellis, and G. Leslie, Phys. Med. Biol. **33**, 711–722 (1988).
[2] M. A. Franceschini, E. Gratton, and S. Fantini, Opt. Lett. **24**, 829–831 (1999).
[3] A. H. Hielscher, J. R. Mourant, and I. J. Bigio, Appl. Opt. **36**, 125–135 (1997).
[4] J. R. Mourant, J. P. Freyer, A. H. Hielscher, A. A. Eick, D. Shen, and T. M. Johnson, Appl. Opt. **37**, 3586–3593 (1998).
[5] L. Dagdug, G. H. Weiss, and A. H. Gandjbakhche, Phys. Med. Biol. **48**, 1361–1370 (2003).
[6] G. Zaccanti, L. Alianelli, C. Blumetti, and S. Carraresi, Opt. Lett. **24**, 1290–1292 (1999).
[7] R. F. Bonner, R. Nossal, and G. H. Weiss, Photon Migration in Tissues, B. Chance (ed.) (Plenum, New-York, 1998), pp. 11–23.
[8] S. Del Bianco, F. Martelli, and G. Zaccanti, Phys. Med. Biol. **47**, 4131–4144 (2002).
[9] X. Guo, M. F. G. Wood, and A. Vitkin, Opt. Comm. **281**, 380–387 (2008).
[10] Y. Yang, E. J. Celmer, J. A. Koutcher, and R. R. Alfano, J. Clin. Laser. Med. Surg. **19**, 35–39 (2001).
[11] C. Zhu, G. M. Palmer, T. M. Breslin, J. Harter, and N. Ramanujam, Lasers in Surgery and Medicine **38**, 714–724 (2006).
[12] A. E. Cerussi, V. W. Tanamai, D. Hsiang, J. Bulter, R. S. Mehta, and B. J. Tromberg, Phil. Trans. R Soc. A **369**, 4512–4530 (2011).
[13] R. Ankri, V. Peretz, M. Motiei, R. Popovtzer, and D. Fixler, Int. J. Nanomedicine **7**, 449–455 (2012).
[14] R. Ankri, H. Duadi, M. Motiei, and D. Fixler, J Biophotonics **5**, 1–11 (2012).
[15] T. J. Farrell, M. S. Patterson, and B. Wilson, Med. Phys. **19**, 879–788 (1992).
[16] S. T. Jacques, and B. W. Pogue, J. Biomed. Opt. **13**, 0413021–04130219 (2008).
[17] P. K. Jain, K. S. Lee, I. H. El-Sayed, and M. A. El-Sayed, J. Phys. Chem. B **110**, 7238–7248 (2006).
[18] K. Sokolov, J. Aaron, B. Hsu, D. Nida, A. Gillenwater, M. Follen, C. MacAulay, K. Adler-Storthz, B. Korgel, M. Descour, R. Pasqualini, W. Arap, W. Lam, and R. Richards-Kortum, Technol. Cancer Res. Treat **2**, 491–504 (2003).
[19] S. Mallidi, T. Larson, J. Tam, P. P. Joshi, A. Karpiouk, K. Sokolov, and S. Emelianov, Nano Letters **9**, 2825–2831 (2009).
[20] J. M. Tam, J. O. Tam, A. Murthy, D. R. Ingram, L. L. Ma, K. Travis, K. P. Johnston, and K. V. Sokolov, ACS Nano **4**, 2178–2184 (2010).
[21] M. J. Crow, K. Seekell, J. H. Ostrander, and A. Wax, ACS Nano **5**, 8532–8540 (2011).
[22] K. H. Su, Q. H. Wei, X. Zhang, J. J. Mock, D. R. Smith, and S. Schultz, Nano Letters **3**, 1087–1090 (2003).

[23] P. K. Jain, W. Huang, and A. El-Sayed, Nano Letters **7**, 2080–2088 (2007).
[24] S. Mallidi, T. Larson, J. Aaron, K. Sokolov, and S. Emelianov, Optics Express **15**, 6583–6588 (2007).
[25] J. Baselga, Eur. J. Cancer **37**, 16–22 (2001).
[26] R. Ankri, H. Taitelbaum, and D. Fixler, J. Biomed. Opt. **16**, 085001 (2011).
[27] B. Nikoobakht, and M. A. El-Sayed, Chem. Mater **15**, 1957–1962 (2003).
[28] J. S. Dam, C. B. Pedersen, T. Dalgaard, P. E. Fabricius, P. Aruna, and S. Andersson-Engels, Appl. Opt. **40**, 1155–1164 (2001).
[29] R. Cubeddu, A. Pifferi, P. Taroni, A. Torricelli, and G. Valentini, Phys. Med. Biol. **42**, 1971–1979 (1997).
[30] B. T. Draine, and P. J. Flatau, J. Opt. Soc. Am. A **11**, 1491–1499 (1994).
[31] B. T. Draine and P. J. Flatau. User Guide to the Discrete Dipole Approximation Code DDSCAT 7.0. http://arXivorg/abs/10021505 (2004).
[32] H. Chen, X. Kou, Z. Yang, W. Ni, and J. Wang, Langmuir **24**, 5233–5237 (2008).
[33] H. Ding, J. Q. Lu, K. M Jacobs, and X. Hu, JOSA A **22**, 1151–1157 (2005).
[34] H. Li, S. Xie, and L. Lin, Proc. Conf. Lasers and Electrooptics, **3**, 1018–1019 (1999).

